CO_2 Methanation: Optimal Start-Up Control of a Fixed-Bed Reactor for Power-To-Gas Applications

Jens Bremer[1], Karsten H. G. Rätze[1], and Kai Sundmacher[1,2]

[1]Max Planck Institute for Dynamics of Complex Technical Systems, Sandtorstr. 1, 39106 Magdeburg, Germany

[2]Otto-von-Guericke University Magdeburg, Process Systems Engineering, Universitätsplatz 2, 39106 Magdeburg, Germany

Abstract

Utilizing volatile renewable energy sources (e.g., solar, wind) for chemical production systems requires a deeper understanding of their dynamic operation modes. Taking the example of a methanation reactor in the context of power-to-gas applications, a dynamic optimization approach is used to identify control trajectories for a time optimal reactor start-up avoiding distinct hot spot formation. For the optimization, we develop a dynamic, two-dimensional model of a fixed-bed tube reactor for carbon dioxide methanation which is based on the reaction scheme of the underlying exothermic Sabatier reaction mechanism. While controlling dynamic hot spot formation inside the catalyst bed, we prove the applicability of our methodology and investigate the feasibility of dynamic carbon dioxide methanation.

Introduction

An example of current interest in dynamic reactor operation is the utilization of renewable resources for chemicals production. The main challenge in dealing with these resources lies in their volatile nature[1], such that a deeper understanding of dynamic reactor control becomes crucial. Therefore, we explore a typical process route from renewable energy to methane, as shown in Fig. 1. Frequent

reactor load changes can be expected due to the volatility of renewable electricity used for the process (e.g., coming from wind energy). The methanation unit, a catalytic tubular reactor, is very sensitive to volatile inputs coming from a significant heat release during operation, and especially during start-up. For this reason temperature control is of major interest in fixed-bed methanation[2]. However, this reactor type is broadly analyzed under steady state operating conditions[3–6]. More recently, the dynamics of a steady state operation of carbon monoxide methanation have been investigated in terms of step responses for control and system analysis[7]. More relevant within the context of renewables, Güttel[1] investigated the system dynamics with respect to cycling inputs for time periods in the order of seconds, but also just for lab-scale carbon monoxide methanation. Nevertheless, the consideration of an industrial scale reactor is more reasonable on which literature has paid little attention so far. In addition, we see that carbon dioxide is more relevant for the purpose of utilizing volatile renewable energy sources, due to its direct availability from biogas production (see Fig. 1). Assuming such a production scenario, unsteady operation modes (e.g., reactor start-up and shut-down) are occurring more frequently, so that it becomes more relevant to investigate an optimal dynamic operation. In the present work we pursue an optimization methodology to obtain an optimal reactor start-up with a subsequent steady state operation of a carbon dioxide methanation reactor. Our major objective is to avoid distinct hot spot formation together with reducing the time to achieve a steady state. Therefore, we focus on one single reactor tube which is one part of an entire reactor bundle in industrial applications. To meet the quality requirements for synthetic natural gas (SNG) injection into the natural gas grid, several reactor bundles with attached intercoolers or condensation units are connected in series[5,8]. These auxiliary units are not considered in this work; instead we pay attention to the first reactor section of an industrial plant which is the most relevant in terms of heat release and temperature sensitivity. To capture the essential reactor dynamics within its entire interior, we develop a rigorous dynamic two-dimensional fixed-bed reactor model which is controllable via cooling the reactor jacket. In contrast to other concepts (e.g., the adiabatic fixed-bed reactor) the cooled reactor enables a better controllability of conversion and heat release[2] which is necessary within the context of renewable energy integration. More details on the model are given in the next section.

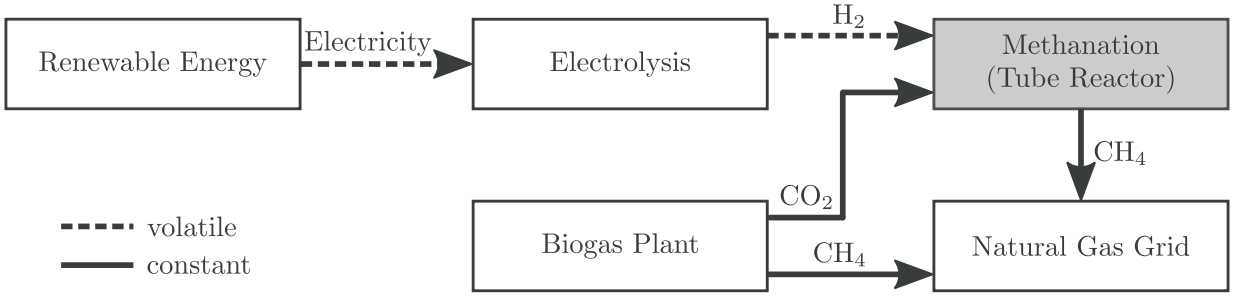

Figure 1: Power-to-gas process route for the conversion of renewable electricity[9]

Reactor Model

The investigated reactor model consists of one single reactor tube. This tube is packed with spherical nickel catalyst particles to promote the carbon dioxide methanation. Among the relevant catalyst materials, nickel is highly active and the most selective material[2]. Furthermore, nickel is very attractive for industrial applications due to its comparatively low price. The reaction scheme for carbon dioxide methanation is given by:

$$\mathrm{CH_4 + H_2O \rightleftharpoons CO + 3\,H_2}, \qquad (\Delta_R \tilde{H}_1^0 = 206.3\ \mathrm{kJ/mol}) \tag{1}$$

$$\mathrm{CO + H_2O \rightleftharpoons CO_2 + H_2}, \qquad (\Delta_R \tilde{H}_2^0 = -41.1\ \mathrm{kJ/mol}) \tag{2}$$

$$\mathrm{CH_4 + 2\,H_2O \rightleftharpoons CO_2 + 4\,H_2}. \qquad (\Delta_R \tilde{H}_3^0 = 164.9\ \mathrm{kJ/mol}) \tag{3}$$

The respective standard reaction enthalpy in reaction (3) highlights the above mentioned drawback of methane generation from hydrogen and carbon dioxide. The exothermic nature results in a high heat release which might cause thermal degradation of the catalyst[10] or rupture of tube materials[11]. Additionally, Jürgensen et al.[4] report significant carbon formation starting at elevated temperatures of 770 K which significantly reduces the catalyst activity. Facing these issues, we consider temperature control at the outer reactor wall as the most promising strategy to ensure stable reactor operation. For further comprehension, Fig. 2 illustrates the reactor tube, showing the dimensions and modeling features. The corresponding numeric values and further reactor specifications are given in Tab. 1. These specifications are chosen to incorporate several studies on carbon dioxide methanation[4–6,8] and to ensure a sufficient carbon dioxide conversion. The heat transfer coefficient k_w is taken from VDI[12] considering the wall thickness δ and the thermo-physical properties of austenitic cast steel as tube material. The catalyst density ρ_{cat} refers to the specifications of Xu and Froment[13]; the catalyst specific heat capacity is taken from Oliveira et al.[14]; the conductivity of the

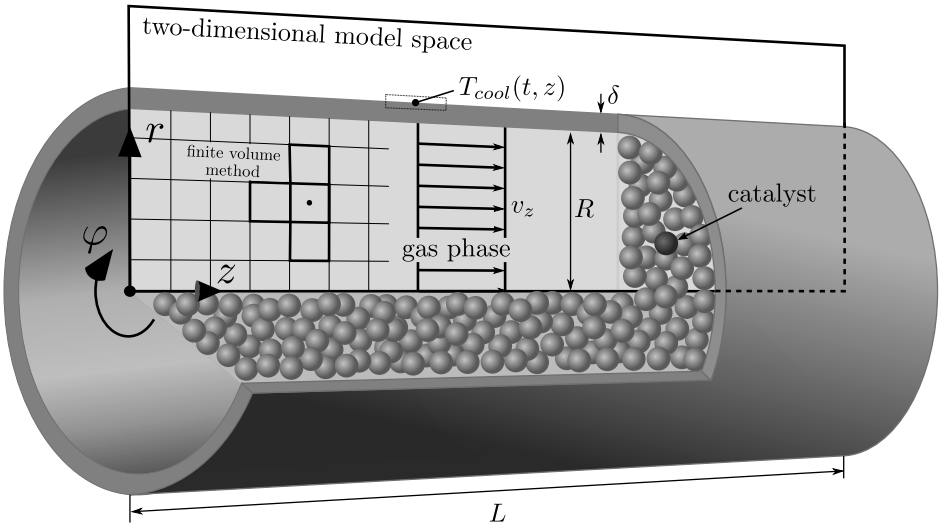

Figure 2: Illustration of the cooled fixed-bed tube reactor

nickel catalyst can be found in De Falco et al.[15].

To enable a detailed analysis of the start-up dynamics over the entire spatial reactor domain a two-dimensional, pseudo-homogeneous, dynamic reactor model for the methanation reactor is derived. Therefore, we apply mass and energy balances over an arbitrary control volume living in a cylindrical coordinate system (see Fig. 2). Since pressure drop due to friction typically dominates a dynamic momentum balance for packed bed reactors[16], this balance is not involved in this study. Instead, the Ergun equation is used to account for the friction term[17]. For further simplification, a constant superficial gas velocity in axial direction v_z and ideal gas behavior is assumed. Although, the underlying Sabatier reaction mechanism is non-equimolar and possibly leads to an increasing gas velocity in axial direction, v_z is included as the respective mean velocity. A more detailed description of the velocity field would certainly increase the model accuracy, but also leads to larger computation times for simulation and in particular for optimization. Furthermore, increasing velocities during the

Table 1: Reactor specifications

reactor radius	R	=	0.01	m
reactor length	L	=	5	m
wall thickness	δ	=	0.02	m
catalyst particle diameter	d_p	=	0.002	m
fixed-bed void fraction	ε	=	0.4	
catalyst density	ρ_{cat}	=	2355.2	kg/m^3
catalyst specific heat capacity	$c_{p,\text{cat}}$	=	1107	J/(kg K)
catalyst emmisivity	ϵ_{cat}	=	0.4	
catalyst conductivity	λ_{cat}	=	0.3489	W/(m K)
heat transfer coefficient	k_w	=	120	W/(m^2 K)

reaction would possibly reduce the absolute hot spot temperature due to enhanced convection, such that our assumption represents a worst case scenario for reactor controllability. Due to the symmetric tube geometry a state change in φ-direction is neglected. Considering these assumptions, the following partial differential equation (PDE) system remains:

$$\frac{\partial \rho_\alpha}{\partial t} = -\frac{v_z}{\varepsilon}\frac{\partial \rho_\alpha}{\partial z} + \frac{\mathcal{D}_{r,\alpha}^{\text{eff}}}{\varepsilon}\left(\frac{\partial^2 \rho_\alpha}{\partial r^2} + \frac{1}{r}\frac{\partial \rho_\alpha}{\partial r}\right) + \frac{1-\varepsilon}{\varepsilon} M_\alpha \sum_\beta \nu_{\alpha,\beta}\, \tilde{r}_\beta, \tag{4}$$

$$\frac{\partial T}{\partial t} = \frac{1}{(\rho c_p)^{\text{eff}}}\left[-\sum_\alpha \rho_\alpha c_{p,\alpha} v_z \frac{\partial T}{\partial z} + \lambda_r^{\text{eff}}\left(\frac{\partial^2 T}{\partial r^2} + \frac{1}{r}\frac{\partial T}{\partial r}\right) - (1-\varepsilon)\sum_\beta \left(\Delta_R \tilde{H}_\beta\right)\tilde{r}_\beta\right], \tag{5}$$

where ρ_α relates to the mass concentration of all five components in reaction $\beta \in [1,2,3]$ and nitrogen as an inert component; v_z originates to the given constant superficial velocity; $\mathcal{D}_{r,\alpha}^{\text{eff}}$ is the effective radial dispersion coefficient of each component; λ_r^{eff} accounts for the effective radial heat conductivity; T is the temperature of the pseudo-homogeneous phase; ε stands for the void fraction of the fixed-bed; M_α is the molar mass of component α; $\nu_{\alpha,\beta}$ is the stoichiometric coefficient of component α in reaction β; $\tilde{r}_\beta$ represents the rate equation for reaction β and $\Delta_R \tilde{H}_\beta$ describes the reaction heat for reaction β. More details on physical properties and correlations are part of the following section.

Physical properties and correlations

Most of the physical parameters in Eqs. (4) and (5) are significantly influenced by temperature, pressure, and composition. Considering this, the presence of strong nonlinear dependencies leads to an increase in model complexity. However, in packed-bed reactor modeling this level of complexity is nonetheless necessary to depict real world behavior.[18]

The first physical parameter which needs to be considered more in detail is the effective radial dispersion coefficient $\mathcal{D}_{r,\alpha}^{\text{eff}}$. To incorporate the influence of the axial convection on the radial diffusion Tsotsas and Schlünder[19] established the following correlation:

$$\mathcal{D}_{r,\alpha}^{\text{eff}} = \left(1 - \sqrt{1-\bar{\varepsilon}}\right)\mathcal{D}_{r,\alpha} + \frac{v_z\, d_p}{8},$$

where the first term accounts for a weighted molecular diffusion and the second term results from cross-mixing effects within the packed-bed. As part of our assumptions the averaged porosity $\bar{\varepsilon}$ equals to the constant ε in Tab. 1. To calculate the radial gas diffusion coefficient $\mathcal{D}_{r,\alpha}$, Kee et al.[20] introduced mixture averaged diffusion coefficients of a species α diffusing into a mixture of other

gases

$$\mathcal{D}_{r,\alpha}(T,p,\rho_\alpha) = \frac{\frac{\rho}{M} - \frac{\rho_\alpha}{M_\alpha}}{\sum\limits_{\substack{j=1 \\ j\neq\alpha}} \frac{\rho_j}{M_j} \frac{1}{\mathcal{D}_{\alpha,j}(T,p)}} \qquad \text{with} \qquad \frac{\rho}{M} = \sum_\alpha \frac{\rho_\alpha}{M_\alpha}.$$

The binary diffusion coefficients are calculated by introducing special diffusion volumes υ_α referring to Fuller et al. [21]

$$\mathcal{D}_{\alpha_1,\alpha_2}(T,p) = \frac{10^{-7}\, T^{1.75} \sqrt{10^3 \left(1/M_{\alpha_1} + 1/M_{\alpha_2}\right)}}{(p/1.01325)\ \left[\sqrt[3]{\upsilon_{\alpha_1}} + \sqrt[3]{\upsilon_{\alpha_2}}\right]^2}.$$

Another relevant physical parameter is the effective volumetric heat capacity

$$(\rho c_p)_{\text{eff}} = (1-\varepsilon)\,\rho_{\text{cat}} c_{p,\text{cat}} + \varepsilon \rho_g c_{p,\text{gas}} \quad \text{with} \quad c_{p,\text{gas}}(T,\rho_\alpha) = \sum_\alpha \frac{\rho_\alpha}{\rho}\, c_{p,\alpha}(T)\ ,$$

which consists of constant parameters (e.g., ε, ρ_{cat}, $c_{p,\text{cat}}$ as stated in Tab. 4) and of the temperature dependent mixed gas heat capacity $c_{p,\text{gas}}(T,\rho_\alpha)$. To evaluate the necessary component heat capacities $c_{p,\alpha}$, a polynomial correlation and its respective parameters are taken from VDI [12].

Since this study considers only one pseudo-homogeneous phase to represent the fixed-bed, heat conduction in radial direction is based on the effective heat conductivity. Bauer and Schlünder [22] combined the influence of the axial convective transport, radiation, and the actual conduction by the following relation:

$$\begin{aligned}
\lambda_{\text{eff},r} &= \lambda_{\text{conv}} + \lambda_{\text{cond},r}, \\
\lambda_{\text{conv}} &= \frac{1.15\,\rho\, v_z\, c_{p,\text{gas}}\, d_p}{8\,\left[2-(1-d_p/R)^2\right]}, \\
\lambda_{\text{cond},r} &= \left(1-\sqrt{1-\varepsilon}\right)\,\left(\lambda_{\text{gas}} + \varepsilon\,\lambda_r\right) + \sqrt{1-\varepsilon}\,\lambda_{rs}, \\
\lambda_r &= 2.27\cdot 10^{-7}\ \frac{\epsilon_{\text{cat}}}{2-\epsilon_{\text{cat}}}\, T^3 \cdot d_p.
\end{aligned}$$

Further details on the parameter λ_{rs} can be found in Bauer and Schlünder [22]. The thermal gas conductivity λ_{gas} is taken from Poling et al. [23]

$$\lambda_{\text{gas}}(T,\rho_\alpha) = \sum_{\alpha_1} \frac{\frac{\rho_{\alpha_1}}{M_{\alpha_1}}\,\lambda_{\alpha_1}(T)}{\sum\limits_{\alpha_2} \frac{\rho_{\alpha_2}}{M_{\alpha_2}}\,\phi_{\alpha_1,\alpha_2}(T)},$$

which is determined by thermal component conductivities λ_α and a dynamic viscosity mixing rule

$$\phi_{\alpha_1,\alpha_2}(T) = \frac{\left[1 + (\eta_{\alpha_1}(T)/\eta_{\alpha_2}(T))^{0.5}(M_{\alpha_2}/M_{\alpha_1})^{0.25}\right]^2}{\sqrt{8\,(1 + M_{\alpha_1}/M_{\alpha_2})}}.$$

The dynamic viscosities η_α and the thermal component conductivities λ_α are again extracted from VDI [12].

The most relevant physical parameters are related to the reaction mechanism for carbon dioxide methanation. The Langmuir-Hinshelwood rate equations developed by Xu and Froment [24] for a nickel-alumina catalyst have been widely used for simulation models [2,5,7]. However, for methanation these kinetics were actually measured within a temperature range of 573 K to 673 K. As a result, they might not be applicable for an entire start-up simulation which features a broader temperature range. Other kinetics as given by Kopyscinski [25] are measured for a lower temperature range but consider fluidized-bed reactors under quasi-isothermal conditions. In addition, all available kinetics are steady state kinetics and might not hold under dynamic operation. Nevertheless, for better comparability this work still makes use of the kinetics developed by Xu and Froment [24]. Accordingly, the rate equations in Eq. (4) and (5) originate from

$$r_1(T, p_\alpha) = \frac{b_1(T)}{p_{H_2}^{2.5}} \left(p_{CH_4} p_{H_2O} - \frac{p_{H_2}^3 p_{CO}}{K_1(T)} \right) \Bigg/ (\mathrm{DEN}(T))^2, \tag{6}$$

$$r_2(T, p_\alpha) = \frac{b_2(T)}{p_{H_2}} \left(p_{CO} p_{H_2O} - \frac{p_{H_2} p_{CO_2}}{K_2(T)} \right) \Bigg/ (\mathrm{DEN}(T))^2, \tag{7}$$

$$r_3(T, p_\alpha) = \frac{b_3(T)}{p_{H_2}^{3.5}} \left(p_{CH_4} p_{H_2O}^2 - \frac{p_{H_2}^4 p_{CO_2}}{K_3(T)} \right) \Bigg/ (\mathrm{DEN}(T))^2, \tag{8}$$

where p_α is the partial pressure of the respective component. It is evaluated by

$$p_\alpha = \frac{\rho_\alpha}{\rho} \frac{M}{M_\alpha} p.$$

The rate coefficients b_β for each reaction β are

$$b_\beta(T) = \mathcal{A}_\beta \exp\left(-\frac{E_\beta}{\mathcal{R}T} \right).$$

Table 2: Kinetic parameters to calculate reaction rates; each pre-exponential factor contains a multiplier of 1.225 (see Xu and Froment [24])

α	Formula	$\mathcal{A}_\alpha$	$[\mathcal{A}_\alpha]$	ΔH_α	$[\Delta H_\alpha]$	β	$\mathcal{A}_\beta$	$[\mathcal{A}_\beta]$	E_β	$[E_\beta]$
1	CH_4	8.15e-4	bar^{-1}	-38.28	$\frac{\mathrm{kJ}}{\mathrm{mol}}$	1	5.176e15	$\frac{\mathrm{kmol\,bar}^{0.5}}{\mathrm{kg_{cat}\,h}}$	240.10	$\frac{\mathrm{kJ}}{\mathrm{mol}}$
2	CO	10.08e-5	bar^{-1}	-70.65	$\frac{\mathrm{kJ}}{\mathrm{mol}}$	2	2.395e06	$\frac{\mathrm{kmol}}{\mathrm{kg_{cat}\,h\,bar}}$	67.13	$\frac{\mathrm{kJ}}{\mathrm{mol}}$
4	H_2O	2.17e 5		88.68	$\frac{\mathrm{kJ}}{\mathrm{mol}}$	3	1.250e15	$\frac{\mathrm{kmol\,bar}^{0.5}}{\mathrm{kg_{cat}\,h}}$	243.90	$\frac{\mathrm{kJ}}{\mathrm{mol}}$
5	H_2	7.50e-9	bar^{-1}	-82.90	$\frac{\mathrm{kJ}}{\mathrm{mol}}$					

DEN is a dimensionless parameter defined as

$$\mathrm{DEN}(T) = 1 + B_{CO}(T)\; p_{CO} + B_{H_2}(T)\; p_{H_2} + B_{CH_4}(T)\; p_{CH_4} + \frac{B_{H_2O}(T)\; p_{H_2O}}{p_{H_2}},$$

where B_α is the respective adsorption constant for CH_4, CO, H_2O and H_2

$$B_\alpha(T) = \mathcal{A}_\alpha \exp\left(-\frac{\Delta H_\alpha}{\mathcal{R}T}\right).$$

The constant kinetic parameters $\mathcal{A}_\beta$, E_β, $\mathcal{A}_\alpha$, ΔH_α are stated in Tab. 2. The temperature dependent equilibrium constants K_1, K_2 and K_3 are based on Gibbs energy minimization and the law of mass action as shown in Poling et al. [23]. Furthermore, the heat of reaction $\Delta_R\tilde{H}_\beta$ in Eq. (5) is obtained by component enthalpies weighted over the respective stoichiometric coefficients. All required heat capacity correlations are again taken from VDI [12].

It is worthwhile to mention that the rate equations as used in our pseudo-homogeneous model do not consider internal and external diffusion resistance of the catalyst particle. So far, these parts of the catalytic reaction mechanism are not sufficiently investigated for fixed-bed carbon dioxide methanation under dynamic operation. Although Kopyscinski [25] reported that mass transfer limitations are negligible at temperatures below 610 K, our study shows that this limit is considerably exceeded inside fixed-bed reactor tubes. In addition, we assume that mass transport into the catalyst particles during reactor start-up underlies a significant temporal delay which can be also seen as an initial transport resistance. Ghouse and Adams [26] proved this behavior by developing a two-dimensional heterogeneous reactor model for steam methane reforming (SMR) which is capable of tracking intra-particle mass and heat transport. However, for our pseudo-homogeneous reactor model we use an effectiveness factor χ of 0.1 as reported by Wesenberg and Svendsen [27] to account for this. Thus, the

catalyst mass related reaction rates in Eqs. (6) - (8) are weighted and, furthermore, converted from kmol/($\mathrm{kg_{cat}}$ h) to mol/($\mathrm{m^3_{cat}}$ s) to be applicable in Eqs. (4) and (5)

$$\tilde{r}_\beta = \chi \; r_\beta \; \rho_{\mathrm{cat}} \; 1000 \,/\, 3600.$$

Boundary conditions

Due to symmetry at the central axis, heat transfer across the reactor wall, and feed conditions at the inlet side the respective boundary conditions are:

$$\begin{aligned}
&\rho_\alpha|_{z=0} = \rho_{\alpha,\mathrm{in}} \;, && \left.\frac{\partial \rho_\alpha}{\partial r}\right|_{r=0} = 0 \;, && \left.\frac{\partial \rho_\alpha}{\partial r}\right|_{r=R} = 0 \;, \\
&T|_{z=0} = T_{\mathrm{in}} \;, && \left.\frac{\partial T}{\partial r}\right|_{r=0} = 0 \;, && \left.\frac{\partial T}{\partial r}\right|_{r=R} = \frac{k_w}{\lambda_r^{\mathrm{eff}}|_{r=R}} \left(T_{\mathrm{cool}} - T|_{r=R}\right) \;,
\end{aligned}$$

where k_w is the wall heat transfer coefficient, and T_{cool} represents the cooling temperature at the surface of the outer reactor wall (see Fig. 2). This cooling temperature is further used as control to reach the objective of the optimal control problem formulated in the next section. Since T_{cool} is a function of time and a function of the axial coordinate, the respective control domain would be computationally challenging. Thus, we only focus on the cooling temperature at the inlet and outlet side of the reactor. In between, the cooling temperature follows a linear relationship given by:

$$T_{\mathrm{cool}}(t,z) = (1 - \frac{z}{L}) \; T_{\mathrm{cool,in}}(t) + \frac{z}{L} \; T_{\mathrm{cool,out}}(t).$$

Solution strategy

We discretize the governing PDEs in Eqs. (4) and (5) within the reactor half-plane, using the finite volume method (FVM) as illustrated in Fig. 2, and obtain ordinary differential equations (ODEs). Therefore we use a piecewise constant axial approximation following the upwind scheme and a piecewise linear radial approximation with central differences. One advantage of the FVM is its conservative nature which forces each finite volume (FV) to obey the underlying conservation laws. This might be one reason for FVM to be very accurate even if other common methods (e.g., orthogonal collocation) are possibly faster in terms of computation time[28]. Especially, a large number of finite volumes is certainly preferable in terms of accuracy but unfavorable for computational costs, which is even more distinct in optimization tasks. Based on our experience, we found a resolution of

$n_z = 16$ axial and $n_r = 5$ radial finite volumes to be suitable. In radial direction all FVs are equally distributed; in axial direction the FV size increases logarithmically from 59 mm to 872 mm. This non equidistant meshing incorporates for steep spatial gradients at the reactor inlet side. More detailed discussions on the influence of mesh density is part of the next subsection. Considering all six mass balances and one energy balance (all in all seven PDEs) gives rise to the following nonlinear ODE system of order $n = 16 \cdot 5 \cdot 7 = 560$:

$$\dot{\boldsymbol{x}}(t) = \boldsymbol{f}(\boldsymbol{x}(t), \boldsymbol{u}(t)) \quad \text{with} \quad \boldsymbol{x}(t_0) = \boldsymbol{x}_0, \tag{9}$$

where $\boldsymbol{x}(t) \in \mathbb{R}^n$ is the differential state vector, containing all component mass concentrations and temperatures in all finite volumes. The input vector $\boldsymbol{u}(t) \in \mathbb{R}^2$ contains the controlled cooling temperatures $T_{\text{cool,in}}$ and $T_{\text{cool,out}}$ as mentioned above. The vector function $\boldsymbol{f} : \mathbb{R}^{n+2} \rightarrow \mathbb{R}^n$ contains all relations as stated in the upper sections.

All model parameters and correlations were implemented in Matlab. In addition, we combine the Matlab reactor model with CasADi v3.0.0, a symbolic framework for algorithmic differentiation and numeric optimization developed by Andersson[29]. For integration and dynamic optimization, we make use of a simultaneous optimization strategy realized by orthogonal collocation of the remaining time coordinate. Hence, we obtain a large-scale nonlinear program (NLP) which is solved by IPOPT v3.11[30] incorporated with the MA97 linear solver[31]. More details about the optimization objective used in this work are given in the following section.

Mesh analysis

To identify a sufficient mesh resolution, several start-up simulations are performed with the specifications given in Tab. 4. Therefore, we mainly focus on the maximal temperature (hot spot temperature) which occurs when the reactor starts up with a constant cooling temperature of 650 K. Tab. 3 highlights the results for meshes with up to 1000 FVs. As shown in Tab. 3 the largest impact associates with the number of axial FVs. Our selected mesh (5 radial and 16 axial FVs) is capable of representing the hot spot temperature within an error bound of only 2 percent compared to the highest resolution. A more detailed comparison of these two cases is shown in Fig. 3. Both cases feature a comparable dynamic and spatial trend, such that the chosen mesh for optimization represents a reasonable trade-off between accuracy and computational complexity.

Table 3: Hot spot temperature in K with respect to FV mesh resolution; in brackets - percentage of hot spot temperature compared to high resolution mesh (underlined); bold - mesh used for dynamic optimization.

		Number of axial FVs				
		10	16	20	30	40
Number of radial FVs	5	927.3 (95.8)	**949.8 (98.1)**	954.1 (98.6)	965.2 (99.7)	967.3 (100)
	15	928.0 (95.9)	950.2 (98.2)	954.9 (98.7)	965.5 (99.8)	967.7 (100)
	25	928.2 (95.9)	950.4 (98.2)	955.1 (98.7)	965.6 (99.8)	967.8 (100)

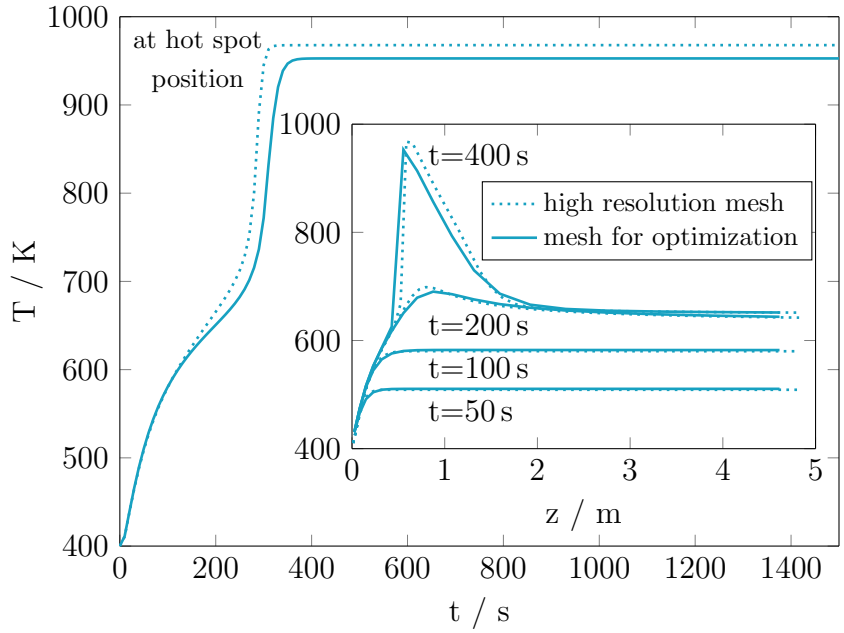

Figure 3: Influence of FV mesh density on reactor temperature development for reactor start-up with constant cooling temperature (650 K); all values at inner reactor axis; 550 CPU seconds for high resolution and 50 CPU seconds for optimization mesh

Dynamic Optimization

We assume a start-up operation case which is determined by inlet conditions and limits on states and controls as highlighted in Tab. 4. Furthermore, we assume a stoichiometric inlet ratio of 4:1 between hydrogen and carbon dioxide to ensure that the catalytic reaction leads to the highest possible temperature increase inside the reactor (worst-case scenario in terms of temperature control). The inlet pressure p_{in} and the gas velocity v_z relates to investigations on optimal plant design reported by El-Sibai et al. [5]. Since the elevated inlet pressure is considered to be a result of an upstream compression unit, the inlet is chosen to be above ambient temperature. Bounding the reactor temperature over the entire interior is of major importance to guarantee long-term stable operation. Referring to Zhang et al. [10], temperatures above 770 K have to be avoided to prevent thermal degradation. A similar bound with respect to carbon formation is stated by Jürgensen et al. [4]. Taking an additional margin of safety into consideration, our selected upper reactor temperature bound is 750 K. Due to the exothermic reaction, the lower reactor temperature bound is not relevant, but quoted for consistency. In contrast, the cooling temperature bounds are result of our observations for the reactor controllability.

The reactor start-up is initiated by a step change in the cooling temperature chosen by the optimizer while the initial reactor bulk gas phase is assumed to be equal to the inlet gas condition:

$$T_{\text{init}}(r,z) = T_{\text{in}}, \qquad p_{\text{init}}(r,z) = p_{\text{in}}, \qquad x_{\alpha,\text{init}}(r,z) = x_{\alpha,\text{in}}. \tag{10}$$

Choosing other initial conditions leads to a significantly larger computation time or even prevents a successful convergence of the solution. Based on these specifications, we define the following dynamic

Table 4: Start-up operation parameters

superficial gas velocity	v_z	=	1	m/s
inlet gas temperature	T_{in}	=	400	K
inlet pressure	p_{in}	=	$5 \cdot 10^5$	Pa
H_2 inlet mole fraction	$x_{\text{H}_2,\text{in}}$	=	0.8	
CO_2 inlet mole fraction	$x_{\text{CO}_2,\text{in}}$	=	0.2	
remaining components inlet mole fraction	$x_{\alpha,\text{in}}$	=	10^{-5}	
upper cooling temperature bound	$T_{\text{cool,ub}}$	=	650	K
lower cooling temperature bound	$T_{\text{cool,lb}}$	=	300	K
upper reactor temperature bound	T_{ub}	=	750	K
lower reactor temperature bound	T_{lb}	=	300	K
start-up time horizon	t_f	=	1000	s

optimization problem:

$$\begin{aligned} \max_{\mathbf{u}(t)} \quad & \int_0^{t_f} X_{CO_2}(\mathbf{x}(t), \mathbf{u}(t))\ dt\ -\ R(\mathbf{u}(t)), \\ \text{s.t.} \quad & \dot{\boldsymbol{x}}(t) = \boldsymbol{f}(\boldsymbol{x}(t), \boldsymbol{u}(t)), \quad \forall t \in [0\ t_f], \\ & \mathbf{x}(0) = \mathbf{x}_0, \\ & \mathbf{x}_{\text{ub}} \geq \mathbf{x} \geq \mathbf{x}_{\text{lb}}, \quad \mathbf{u}_{\text{ub}} \geq \mathbf{u} \geq \mathbf{u}_{\text{lb}}, \end{aligned} \tag{11}$$

where we embed the ODE system in Eq. (9) into a maximization task of the carbon dioxide conversion over the entire start-up time horizon. We consider the Lagrange representation of the maximization of the carbon dioxide conversion to be equivalent to a time minimal start-up objective. Therefore, we use the general definition for the conversion of a continuous process and consider carbon dioxide as reactant

$$X_{CO_2}(t) = 1 - \frac{\dot{n}_{\text{CO}_2,\text{out}}(t)}{\dot{n}_{\text{CO}_2,\text{in}}(t)},$$

where $\dot{n}_{\text{CO}_2,\text{out}}$ is the outlet molar flow rate of carbon dioxide originating from the solution of the ODE system. The inlet molar flow rate $\dot{n}_{\text{CO}_2,\text{in}}$ is a fixed parameter resulting from Tab. 4. In addition, we define the methane selectivity with respect to reaction 3

$$S_{CH_4}(t) = \frac{\dot{n}_{\text{CH}_4,\text{out}}(t) - \dot{n}_{\text{CH}_4,\text{in}}(t)}{\dot{n}_{\text{CO}_2,\text{in}}(t) - \dot{n}_{\text{CO}_2,\text{out}}(t)}.$$

The optimization objective turns out to be highly sensitive to the chosen control which can lead to severe fluctuations in the optimal control trajectories. This computational challenge is directly connected to the physical properties of the exothermic reaction system and its fast kinetics. To face this challenge and to achieve solutions relevant for technical applications, we add a penalty term R to the objective which regularizes the control fluctuations in the following manner:

$$R(\mathbf{u}(t)) = \mathbf{w}^T \sum_{i=1}^{n_\text{c}-1} \left(\mathbf{u}(t_{i+1}) - \mathbf{u}(t_i)\right)^2, \quad t_0 \leq \cdots \leq t_{i-1} \leq t_i \leq t_{i+1} \leq \cdots \leq t_f$$

where $\mathbf{w} \in \mathbb{R}^2$ is a constant penalty factor and n_c relates to the number of available time points. After reformulation of Eq. (11) to a fully discretized NLP, these time points correspond to the chosen collocation points. However, the penalty term affects the objective function and thus also the optimal solution. To avoid the penalty term to superimpose the actual objective, a sensitivity study on this term relating to our optimization setup yields an appropriate factor of $\mathbf{w}^T = [0.001\ 0.001]$. The bounds on controls and on differential states in Eq. (11) are selected to fulfill the technical

requirements in Tab. 4.

As mentioned in the previous section, we make use of a simultaneous approach in order to solve the dynamic optimization problem. Therefore, states and controls are discretized into 40 equidistant finite elements within the start-up time horizon (see Tab. 4). Inside one finite element Lagrange polynomials approximate the state trajectories with three collocation points. Control trajectories are considered to be piecewise constant from one collocation point to another. Thus, differential states vanish and the remaining NLP consists only of algebraic equality and inequality constrains. More details on this methodology are elaborated in a comprehensive overview by Biegler [32].

Results

To evaluate our dynamic optimization results, we compare the NLP solution, an unconstrained start-up simulation with fixed cooling temperatures of 650 K, and an unconstrained start-up simulation with fixed cooling temperatures equal to the steady state solution of the dynamic optimization ($T_{\mathrm{cool,in}} = 517\,\mathrm{K}\,; T_{\mathrm{cool,out}} = 650\,\mathrm{K}$). The unconstrained simulations represent limiting scenarios which do not consider the actual reactor dynamics. All scenarios are highlighted in Fig. 4 with respect to the carbon dioxide conversion, the methane selectivity and the optimal control trajectories during the entire start-up horizon. The dynamic optimization takes 1.4 CPU hours to compute, while the competitive simulations are solved in approx. 50 CPU seconds.

First of all, Fig. 4 illustrates that methane selectivity is very close to one since the carbon monoxide formation due to the chemical equilibrium mostly occurs above 800 K at elevated pressures [2,33,34]. Nevertheless, the reaction rates for carbon monoxide formation dominate at lower temperatures, which gives rise to a lower methane selectivity within the first 100 s. In addition, this early selectivity is also influenced by small initial amounts of methane and carbon monoxide (see Tab. 4 and Eq. (10)). However, once the hot spot is developed, the temperature is high enough such that the equilibrium superimposes kinetic limitations. Thus, conversion appears to be a more reasonable objective due to its higher sensitivity regarding the optimal operation temperature. Furthermore, it can be seen that after approximately 100 s the optimal solution features a reduction of the carbon dioxide conversion which is realized by a decrease of the inlet-side cooling temperature. This decision becomes reasonable, if the reactor temperature development over time is taken into consideration. Therefore, Fig. 5 illustrates the spatial temperature distribution at four different time points.

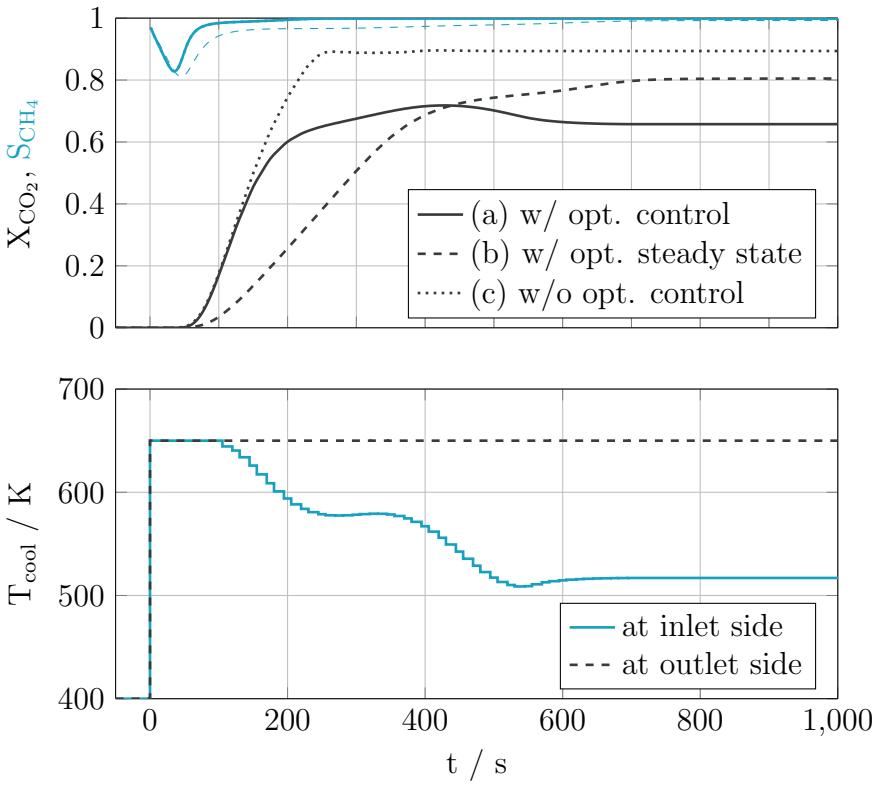

Figure 4: Top: Carbon dioxide conversion and methane selectivity for controlled (a) and uncontrolled (b,c) hot spot formation; Bottom: Control trajectories for (a).

Initially, the optimizer chooses a step change to the highest cooling temperature. At this stage the cooling rather acts as a heating to initiate the catalytic reaction. At 180 s a clear elevation of the reactor temperature due to an advanced conversion is observed. Although, until that time in scenario (a) no bounds of the inner temperature are active, the optimizer already reduces the inlet cooling temperature to counteract the later exothermic heat release. At 550 s the highest inner temperature reaches the bound of 750 K and stays at that temperature until a steady state appears. From this time on, there is a distinct radial dependency that proves the importance of a two-dimensional model setup. In addition, we see the highest temperature right at the central reactor axis which is due to the enhanced heat transport resistance in the center of the packed-bed. As a result of the gas residence time and the thermal inertia of the reactor, we observe that the first control action is approx. 450 s before the maximal reactor temperature is reached. Considering the gas velocity in Tab. 4, the gas residence time of 5 s is significantly smaller than the observed time delay which proves that the thermal inertia is much more relevant for optimal dynamic reactor operation. In the uncontrolled start-up scenario (b) with a cooling temperature of 650 K, an unmistakable increase of the reactor temperature is visible and leads to temperatures of approx. 950 K (equivalent to the scenario used

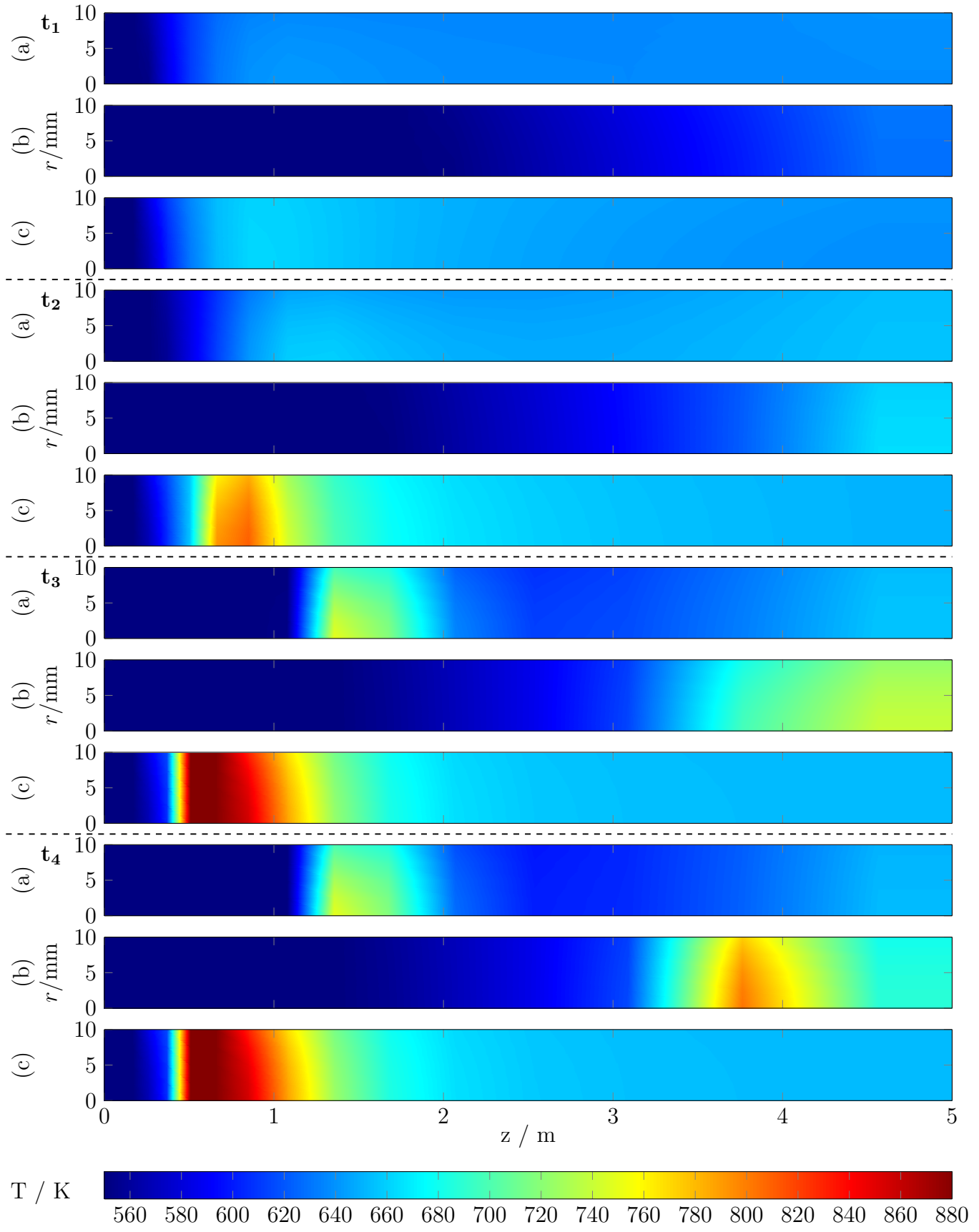

Figure 5: Controlled (a) and uncontrolled reactor temperature distribution with $T_{\text{cool,in}} = 517\,\text{K}$, $T_{\text{cool,out}} = 650\,\text{K}$ (b) and $T_{\text{cool,in}} = T_{\text{cool,out}} = T_{\text{cool,ub}}$ (c); $t_1 = 180\,\text{s}$, $t_2 = 250\,\text{s}$, $t_3 = 550\,\text{s}$, t_4 - steady state.

in Fig. 3). This drastically exceeds our defined bounds and proves the importance of our proposed methodology for optimal start-up operation. An obvious approach might be a steady state control optimization and subsequently using the resulting cooling temperature for reactor start-up. However, the steady state cooling temperatures taken from the dynamic optimization (scenario a) also lead to a violation of our defined bounds (scenario c). The reason for this behavior lies in a slower reactor start-up with an associated slower temperature increase of the fixed bed, such that the hot spot moves towards the warmer reactor outlet. In case of the dynamic optimization the hot spot ignition occurs already close to the reactor inlet due to the high cooling temperatures in the first 100 s. This also shows that the reactor steady state is highly influenced by its previous dynamics, which is often noted as steady state multiplicity. In this context, further start-up scenarios beside step changes (e.g., ramping) might be also possible for future investigations to control the hot spot position within the fixed bed.

These results underline the relevance of optimal control to guarantee a stable dynamic operation of carbon dioxide methanation. Nevertheless, the optimal solution strongly relates to the model assumptions we made in the previous section. In this regard, it might be difficult to change the cooling fluid temperature fast enough to follow the proposed wall temperatures. Therefore, the penalty term could be used to account for possible control inertia. In addition, the thermal inertia of the reactor jacket, which is not considered so far, certainly delays the heat removal depending on the wall thickness. Nevertheless, the general feasibility for temperature control and the dynamic behavior of the reactor interior maintains.

Conclusion

It was shown that our methodology for optimal reactor start-up control is feasible and provides useful knowledge about the dynamics of a carbon dioxide methanation reactor. Furthermore, we provide a dynamic two-dimensional reactor model suitable for simulation and further dynamic optimization tasks. The proposed model is also adaptable to consider fluctuations or disturbances during a continuous operation which opens many other objectives for utilizing renewable energy for dynamic methanation. In addition, it needs to be underlined that the proposed model can also be used for other applications of heterogeneous catalytic gas phase reactions. The major difference is often just given by the underlying rate equations which are very easy to substitute. For instance, the proposed

reactor model can be directly used for steam methane reforming due to its equivalent reaction kinetics. Nevertheless, there is always the need for experimental validation to prove the applicability to real world problems. Although, with increasing model fidelity an experimental validation becomes very complex. For example, measuring the temperature in radial direction as shown in Fig. 5 inside the relatively thin reactor unit might be very challenging. However, model based solutions are often very helpful to understand the principal system behavior, as shown for the optimal reactor start-up in this work.

For future work a more detailed consideration of the cooling jacket and the cooling medium will be of major interest to get closer to real-world applications. Another important objective is the reduction of computational costs to allow for on-line optimization applications, such as nonlinear model predictive control. One important concept in this context might be model order reduction[9] which appears to be very promising, especially for spatially distributed PDE constrained optimization problems.

Acknowledgment

The author Jens Bremer is also affiliated to the "International Max Planck Research School (IMPRS) for Advanced Methods in Process and Systems Engineering (Magdeburg)".

List of Figures

List of Tables

Literature Cited

1. Güttel, R.. Study of unsteady-state operation of methanation by modeling and simulation. *Chemical Engineering & Technology*. 2013;36(10):1675–1682.

2. Rönsch, S., Schneider, J., Matthischke, S., Schlüter, M., Götz, M., Lefebvre, J., Prabhakaran, P., Bajohr, S.. Review on methanation - From fundamentals to current projects. *Fuel*. 2016;166:276 – 296.

3. Parlikkad, N.R., Chambrey, S., Fongarland, P., Fatah, N., Khodakov, A., Capela, S., Guerrini, O.. Modeling of fixed bed methanation reactor for syngas production: Operating window and performance characteristics. *Fuel*. 2013;107:254 – 260.

4. Jürgensen, L., Ehimen, E.A., Born, J., Holm-Nielsen, J.B.. Dynamic biogas upgrading based on the Sabatier process: thermodynamic and dynamic process simulation. *Bioresource technology*. 2015;178:323–329.

5. El-Sibai, A., Rihko-Struckmann, L., Sundmacher, K.. Synthetic methane from CO2: Dynamic optimization of the Sabatier process for power-to-gas applications. In: *12th International Symposium on Process Systems Engineering (PSE) & 25th European Symposium on Computer Aided Process Engineering (ESCAPE)*. 2015:1157–1162.

6. Schlereth, D., Hinrichsen, O.. A fixed-bed reactor modeling study on the methanation of CO2. *Chemical Engineering Research and Design*. 2014;92(4):702–712.

7. Li, X., Yang, B., Zhang, Y.. Dynamics and control study on the low temperature methanation reactor with mass and heat recycle. *Journal of Process Control*. 2013;23(10):1360–1370.

8. Rönsch, S., Matthischke, S., Müller, M., Eichler, P.. Dynamische Simulation von Reaktoren zur Festbettmethanisierung. *Chemie Ingenieur Technik*. 2014;86(8):1198–1204.

9. Bremer, J., Goyal, P., Feng, L., Benner, P., Sundmacher, K.. Nonlinear model order reduction for catalytic tubular reactors. In: *26th European Symposium on Computer Aided Process Engineering*; vol. 38 of *Computer Aided Chemical Engineering*. Elsevier; 2016:2373 – 2378.

10. Zhang, G., Sun, T., Peng, J., Wang, S., Wang, S.. A comparison of Ni/SiC and Ni/Al2O3 catalyzed total methanation for production of synthetic natural gas. *Applied Catalysis A: General*. 2013;462 463:75 – 81.

11. Brightling, J., Farnell, P., Foster, C., Beyer, F.. Steam reforming - 50 years of development and the challenges for the next 50 years. vol. 46. 2005:190–201.

12. VDI, . VDI Heat Atlas. VDI-Buch; Springer Berlin Heidelberg; 2010.

13. Xu, J., Froment, G.F.. Methane steam reforming: II. Diffusional limitations and reactor simulation. *AIChE Journal*. 1989;35(1):97–103.

14. Oliveira, E.L., Grande, C.A., Rodrigues, A.E.. Methane steam reforming in large pore catalyst. *Chemical Engineering Science*. 2010;65(5):1539–1550.

15. De Falco, M., Di Paola, L., Marrelli, L.. Heat transfer and hydrogen permeability in modelling industrial membrane reactors for methane steam reforming. *International Journal of Hydrogen Energy*. 2007;32(14):2902–2913.

16. Adams, T.A., Barton, P.I.. A dynamic two-dimensional heterogeneous model for water gas shift reactors. *International Journal of Hydrogen Energy*. 2009;34(21):8877–8891.

17. Fogler, H.. Elements of Chemical Reaction Engineering. Prentice Hall International Series in the Physical and Chemi; Pearson Education; 2016.

18. Esche, E., Arellano-Garcia, H., Biegler, L.. Optimal operation of a membrane reactor network. *AIChE Journal*. 2014;60(1):170–180.

19. Tsotsas, E., Schlünder, E.. On axial dispersion in packed beds with fluid flow: Über die axiale Dispersion in durchströmten Festbetten. *Chemical Engineering and Processing: Process Intensification*. 1988;24(1):15–31.

20. Kee, R., Coltrin, M., Glarborg, P.. Chemically Reacting Flow: Theory and Practice. Wiley; 2005.

21. Fuller, E.N., Schettler, P.D., Giddins, J.C.. A new method for prediction of binary gas-phase diffusion coefficients. *Industrial And Engineering Chemistry*. 1966;58(5):18 – 27.

22. Bauer, R., Schlünder, E.U.. Effective radial thermal conductivity of packing in gas flow. Part II. Thermal conductivity of the packing fraction without gas flow. *Int Chem Eng*. 1978;18(2):189 – 204.

23. Poling, B.E., Prausnitz, J.M., O'Connell, J.P.. The Properties of Gases and Liquids. McGraw-Hill; 2001.

24. Xu, J., Froment, G.F.. Methane steam reforming, methanation and water-gas shift: I. intrinsic kinetics. *AIChE Journal*. 1989;35(1):88–96.

25. Kopyscinski, J.. Production of synthetic natural gas in a fluidized bed reactor. Ph.D. thesis; ETH Zürich; 2010.

26. Ghouse, J.H., Adams, T.A.. A multi-scale dynamic two-dimensional heterogeneous model for catalytic steam methane reforming reactors. *International Journal of Hydrogen Energy*. 2013;38(24):9984–9999.

27. Wesenberg, M.H., Svendsen, H.F.. Mass and heat transfer limitations in a heterogeneous model of a gas-heated steam reformer. *Industrial & Engineering Chemistry Research*. 2007;46(3):667–676.

28. Nashtaee, P.S., Khoshandam, B.. Noncatalytic gas-solid reactions in packed bed reactors: a comparison between numerical and approximate solution techniques. *Chemical Engineering Communications*. 2014;201(1):120–152.

29. Andersson, J.. A General-Purpose Software Framework for Dynamic Optimization. PhD thesis; Arenberg Doctoral School, KU Leuven; Department of Electrical Engineering (ESAT/SCD) and Optimization in Engineering Center, Kasteelpark Arenberg 10, 3001-Heverlee, Belgium; 2013.

30. Wächter, A., Biegler, L.T.. On the implementation of an interior-point filter line-search algorithm for large-scale nonlinear programming. *Mathematical programming*. 2006;106(1):25–57.

31. HSL, . A collection of fortran codes for large-scale scientific computation. 2007.

32. Biegler, L.T.. An overview of simultaneous strategies for dynamic optimization. *Chemical Engineering and Processing: Process Intensification*. 2007;46(11):1043 – 1053. Special Issue on Process Optimization and Control in Chemical Engineering and Processing.

33. Gao, J., Wang, Y., Ping, Y., Hu, D., Xu, G., Gu, F., Su, F.. A thermodynamic analysis of methanation reactions of carbon oxides for the production of synthetic natural gas. *RSC Advances*. 2012;2(6):2358–2368.

34. Kiewidt, L., Thöming, J.. Predicting optimal temperature profiles in single-stage fixed-bed reactors for CO2-methanation. *Chemical Engineering Science*. 2015;132:59–71.